Single track formation of pure copper in directed energy deposition using a blue laser

Mitsugu Yamaguchi (yamaguchi@se.kanazawa-u.ac.jp)
Advanced Manufacturing Technology Institute, Kanazawa University https://orcid.org/0000-0001-6034-3089
Masamichi Yamazaki
Yoshinori Funada
Taisei Yachi
Ayahito Saikai
Tatsuaki Furmoto

Research Article

Keywords: additive manufacturing, directed energy deposition, pure copper, semiconductor blue laser, stainless steel

Posted Date: March 8th, 2022

DOI: https://doi.org/10.21203/rs.3.rs-1406173/v1

Abstract

Additive manufacturing (AM) techniques, including directed energy deposition (DED), have been developed and applied in the copper parts manufacturing. DED processes with conventional infrared lasers require more energy owing to the low laser absorptivity of copper. Moreover, local thermal gradients cause large residual stresses, resulting in cracks, deformation, and failure of parts. This study focused on the DED process of pure copper using a blue laser with a wavelength of 445 nm and addressed the following deficiencies. Firstly, the influence of process parameters on the geometry and surface defects of the built structure, such as meandering, distortion, and cracking, were investigated. Secondly, the chemical composition of cross-sections of the built structure was analyzed using an electron probe microanalyzer (EPMA). Finally, a prediction of surface defect-free building conditions was presented. The results indicated that the laser power directly affected the built width and penetration depth, while the built height varied with the rate of powder supplied, and that the traverse speed was inversely proportional to the built height and width. The meandering and distortion of the built structure may be attributed to changes in the melting of the powder and process instability due to obstructions in the optical path of the laser. Meanwhile, the cracks generated owing to shrinkage during solidification when the molten area was formed by laser irradiation are insufficient. A structure without defects can be obtained at a powder feed rate of 20 mg/s, laser power between 60–270 W, and traverse speeds between 10–20 mm/s.

1. Introduction

With regards to global environmental problems, the need for functional materials that offer diverse material properties, weight optimization, and cost reduction is paramount. Among these materials, copper-stainless steel hybrid structures are promising as they can simultaneously utilize the high thermal/electrical conductivity of copper as well as the high mechanical strength, corrosion, and oxidation resistance of stainless steel [1]. These properties are useful in power generation, nuclear, heat exchanger, automotive, and electronic component industries [2-4]. Meanwhile, additive manufacturing (AM) techniques, such aspowder bed fusion (PBF), directed energy deposition (DED), binder jetting (BJ), and cold spray (CS), have been developed and applied in the manufacturing of metallic parts [5]. It is necessary to select an appropriate technique that varies according to the size and complexity of the building part to fully demonstrate the ability of the AM process. AM is a promising technology for manufacturing complex structures with acceptable mechanical properties and high efficiency. Previous studies have reported the following issues regarding the AM of copper parts: Zhang et al. [6] focused on the DED process of pure copper on H13 tool steel using a continuous wave (CW) ytterbium (Yb) fiber laser with a wavelength of 1064 nm and showed that cracks were generated in the bonded area. This was attributed to differences in the thermal expansion coefficients. Moreover, they reported that defect-free deposition of pure copper on stainless steel was achieved using a nickel-based alloy as an intermediate layer [7]. Sun et al. [8] evaluated the boundary of a pure copper/stainless steel interface fabricated via the PBF process using a Yb fiber laser with a wavelength of 1064 nm and revealed that the steel-rich

precipitates were unevenly distributed at the boundary. In the PBF and DED processes using a conventional infrared laser with a wavelength of approximately 1 μm, the required energy was much higher because of its low laser absorptivity. [9]. In addition, owing to the rapid melting/solidification of copper powder, local thermal gradients can produce large residual stresses that are related to the difference in thermal conductivity and thermal expansion coefficient between copper and stainless steel. This results in cracking, deformation, and failure of the parts. Meanwhile, many studies on the CS and BJ processes have been conducted. Huang et al. [10] investigated the properties of a pure copper buildup on a preheated stainlesssteel substrate during the CS process and compared the results with those obtained using the PBF process. They indicated that the microstructure of the built part obtained via the PBF process consisted of polycrystalline grains with substructures including columnar dendrites and equiaxed structures, although the microstructure via the CS process was only equiaxed grains. They also showed that the electrical conductivity of the built part via the CS process was higher than that via the PBF process. Adamson et al. [11] evaluated the residual stress distribution inside a deposited pure copper part on an aluminum substrate via the CS process. It was concluded that the residual stress obtained via the CS process was not as large as compared to that obtained via the PBF process, and the CS process was advantageous in terms of the high deposition rate and low deposition temperature. Hutasoit et al. [12] investigated the influence of building orientation and heat treatment of the built part obtained via the CS process on the mechanical properties. They demonstrated that the formation of porosity varied depending on the building orientation; even though annealing treatment of the as-built part improved the tensile strength, the annealing treatment could not eliminate the porosity. Miyanaji et al. [13] proposed building a porous structure using a mixture of pure copper and copper oxide powder via the BJ process to form high porosity parts and showed that a high-porosity structure was achieved with a sintering atmosphere. They also showed that the use of fine pure copper powder with a median particle size of 10 μm for the BJ process improved the sintered density and tensile stress [14]. The BJ process requires low power to fabricate green parts, but post-processing such as green part curing, debinding, and sintering is required to complete the final parts [15]. In the CS and BJ processes, one of the challenges is the low density and high porosity of the built parts, which require further post-processing such as hot isostatic pressing (HIP) to obtain dense parts. Moreover, the built parts fabricated using CS have very little ductility in the as-sprayed condition [16].

The functional and mechanical performances of the copper parts can be influenced not only by the process parameters, but also by a range of properties that are associated with the powdered material. One of the intrinsic parameters is the laser absorptivity of the powdered material. Gargalis et al. [17] investigated the absorption characteristics during PBF processes using a Yb fiber laser with a wavelength of 1070 nm through direct calorimetry when pure copper powder was built on a copper substrate. They demonstrated that the absorptivity of copper powder was four times higher than that of the bare material owing to the decrease in the threshold required to melt the materials in the presence of copper powder, and the building quality was improved by the increase in effective absorptivity of the copper powder. Yadav et al. [18] performed the DED process of pure copper on stainless steel using a frequency-doubled disk laser with an effective wavelength of 515 nm to identify the process parameter window for the

multilayer building and revealed that the principal factor affecting the building quality of pure copper was the laser energy supplied to the feed powder. They also reported that the construction of a copper-nickel graded multi-layer using a CW fiber laser was achieved by heating the substrate up to 250°C [19]. Yasuda et al. [20] revealed that higher laser power can promote necking between copper particles, and blue laser sintering successively suppresses the oxidation of copper. Ono et al. [21] focused on the DED process of pure copper using a blue laser and showed that the cross-sectional area of the rods increased significantly with an increase in the laser output power, although the cross-sectional area of the rods increased slightly with an increase in the powder feed rate. When the laser power was 30 W, the surface of the built part was not oxidized because the rod cooled immediately after solidification. It was concluded that the reduction in the effect of residual heat due to the amount of heat input forms a high-quality rod. Asano et al. [22] compared the DED process of pure copper on stainless steel using blue and infrared lasers and revealed that the advantage of a blue laser was a lower laser intensity to produce a continuous copper line structure. When the laser intensities were 69 kW/cm^2 for blue lasers and 108 kW/cm^2 for infrared lasers, a structure without voids was obtained. These results indicate that the higher absorptivity of copper to blue lasers can produce a stable copper layer at a low laser power. However, the influence of process parameters on the geometry of the built structure and crack generation during the DED process with a blue laser has not been fully explained. For the process with a laser beam, the interaction between the process parameters and chemical composition is relevant to crack generation [23]. The excellent absorption characteristics of the blue laser can be expected to suppress several factors affecting crack generation, such as excessive expansion of the heat-affected zone and a non-uniform distribution of precipitates at the boundary between the built structure and substrate.

This study focused on the DED-LB/M process of pure copper on stainless steel using a blue laser with a wavelength of 445 nm and addressed the following deficiencies. Firstly, the influences of process parameters, including the laser power and traverse speed, on the geometry and surface defects of the built structure, such as meandering, distortion, and cracks, were investigated. Secondly, the chemical composition of the cross-section of the built structure was analyzed using an electron probe microanalyzer (EPMA). Finally, a prediction of the surface defect-free building condition is presented.

2. Materials And Procedures

Fig. 1 illustrates the experimental setup, and Table 1 lists the experimental conditions. A DED-LB/M machine (Muratani Machine Co. Ltd., ALPION type-BLUE) composed of three semiconductor lasers with a wavelength of 445 nm was used. A focused laser beam with a maximum laser power of 300 W was applied to the surface of the substrate, and a metal powder was supplied through the center of a coaxial nozzle via a shielding flow of argon gas. To investigate the influence of the process parameters on the formation of a single-line track, the laser power and traverse speed were set between 30–270 W and 10–50 mm/s, respectively. The metal powder was pure copper with particle diameters ranging from 31–71 μm (D_{10}-D_{90}), with an average diameter of 46 μm (D_{50}). The substrate was stainless steel (AISI 304) with measurments 50 mm × 50 mm × 5 mm, which was sandblasted by silicon carbide (SiC) abrasive grains

to provide a constant roughness of Ra = 1.56 μm. The height of the built structure was measured using a stylus-type surface roughness tester (Tokyo Seimitsu Co. Ltd., SURFCOM 2000DX2). The width of the built structure was measured using an optical microscope (OM) (Keyence Corp., VHX-6000), and the penetration depth was assessed using cross-sectional observations. The specimens were coarsely ground, polished, and then etched in a chemical etchant containing 10% oxalic acid for 30 s before observing using an OM. The quality of the built structure was evaluated with defects classified as meandering, cracks, or distortions using OM images and cross-sectional profiles, as shown in Figs. 2 and 3. The chemical composition of the cross-section of the built structure was analyzed using an EPMA (JEOL Ltd.,JXA-8530FPlus).

Table 1 Building conditions

Laser source	
Laser type	Semiconductor laser
Wavelength [nm]	445
Laser power [W]	30 - 270
Spot size [mm]	0.2
Traverse speed [mm/s]	10 - 50
Powder feed rate [mg/s]	20
Shielding gas	Ar
Powder	
Material	Pure copper
Average diameter D_{50} [μm]	46
Substrate	
Material	AISI 304
Size [mm] × [mm] × [mm]	50 × 50 × 5

3. Experimental Results And Discussion

3.1. Influence of the laser power on single track formation

Fig. 4 depicts the variation in the built heights, widths, and penetration depths at a traverse speed of 10 mm/s, powder feed rate of 20 mg/s, and various laser powers. The built widths increased linearly, while the penetration depths increased gradually with the laser power. The built heights increased initially as the laser power increased, but reached an upper limit. Because the penetration depth was low for low

laser powers, it seems that the molten powder produced by the laser irradiation was deposited on the substrate, leading to a gradual increase in the built height. Meanwhile, the built height reaches a limit at higher laser powers. This is due to the amount of powder supply remaining constant, even though the width of the penetration area increases as the laser power increases.

3.2. Influence of the traverse speed on single track formation

Fig. 5(a) displays the variation in the built heights and widths at a laser power of 180 W, powder feed rate of 20 mg/s, and various traverse speeds. A comparison of the penetration depths when the powder feed rates are 0 mg/s (i.e., laser irradiation only) and 20 mg/s is shown in Fig. 5(b). The built heights and widths decreased with an increase in the traverse speed. This is because both the powder feed rate and traverse speed are factors that affect the amount of powder supplied per unit area. This means that the amount of powder supplied varies with the traverse speed. Meanwhile, the penetration depth without any powder supply was four times as large as that with a powder supply at a traverse speed of 10 mm/s, but was almost the same when the traverse speed was 50 mm/s. This reveals that the powder supply suppresses the increase in penetration depth, and its effect diminishes at higher traverse speeds. During the DED-LB/M process, the surface of the substrate is melted by laser irradiation; subsequently, the powder is supplied to the molten area in order to obtain the built structure. Because the powder has a lower melting point than the substrate, thermal conduction from the molten metal of the substrate melts the supplied powder.

These results indicate that it is necessary to select a suitable laser power and powder feed rate to obtain the desired geometry and penetration of the built structure.

3.3. Quality assessment of the built structure

The quality of the built structure on a single-line track was evaluated with regards to defects such as meandering, distortions, and cracking.

Fig. 6 presents the appearance of the built structures fabricated at a traverse speed of 40 mm/s, powder feed rate of 20 mg/s, and laser powers of 30 and 240 W. The powder was partially deposited on the substrate at a laser power of 30 W, and a discontinuous structure was obtained. Owing to the lower heat input, the formation of the molten area was insufficient, which contributed to the partial melting and solidification of the powder on the substrate. When the laser power was 240 W, the outline of the built structure was non-uniform, and showed signs of meandering. In addition, metal vapor (i.e., fumes) adhering to the substrate was observed. It has been reported that recoil pressure is generated by evaporation on the surface of the molten metal formed by laser irradiation, which affects the morphology of the melt pool [24, 25]. It is considered that the effects of the recoil pressure on the morphology of the molten metal become significant at higher laser powers. Moreover, the beam quality at the focal position deteriorates owing to the intrusion of metal vapor into the laser's optical path. The interaction between these factors can affect the meandering of the built structure.

Fig. 7 shows a 2D color plot of the proportion of meandering area of the built structure. The meandering area was defined as the ratio of the meandering area measured from the built structure outline to the area surrounded by a straight line along the maximum width of the built structure, as shown in Fig. 2. As the laser power was less than 60 W, the proportion of the meandering area increased. This is because a lower laser power produced a discontinuous structure owing to the lack of heat input, as demonstrated in Fig. 6(a). In contrast, meandering of the built structure was observed at a higher laser power and traverse speed, as displayed in Fig. 6(b). This may be attributed to the interaction between the increase in the recoil pressure and the deterioration of the beam quality due to the intrusion of metal vapor with the increase of the laser power. Meanwhile, the penetration depth decreased with an increase in the traverse speed, as shown in Fig. 5(b). When the penetration size relevant to the heat capacity is small, the effect of thermal conduction from the molten metal of the substrate to the powder weakens. This reveals that the absorption characteristics of the powder are a key factor affecting the melting of the powder at higher traverse speeds. The absorption characteristics vary depending on the chemical composition, particle morphology, and particle size distribution of the powder [26]. Because the powder is constantly supplied from the coaxial nozzle and a laser-irradiated spot on the powder surface changes instantaneously in the DED process, it seems that the melting aspect of the powder varies with the variation in the absorption characteristics relevant to the particle morphology and particle size distribution. As a result, the process is unstable at a higher traverse speed, resulting in the non-uniform geometry of the built structure.

Fig. 8 compares the cross-sectional profiles of the built structures fabricated at a laser power of 180 W and traverse speeds of 20 and 40 mm/s. For a traverse speed of 20 mm/s, a well-formed geometry of the built structure was obtained. Owing to sufficient melting of the powder, the built structure exhibited a semicircular geometry due to the surface tension. Meanwhile, the surface was uneven at a traverse speed of 40 mm/s. The energy density decreases with an increase in the traverse speed, which may produce partially molten and adhered powder on the built surface, resulting in the irregular geometry of the built structure.

Figure 9 depicts a 2D color plot of the amount of surface distortion in the built structure. The amount of distortion increased with an increase in the laser power and traverse speed. The meandering of the built structure and surface distortion may be caused by changes of the powder during melting. When the traverse speed is high, the effect of thermal conduction from the molten metal of the substrate to the powder weakens owing to the small size of the penetration area. Melting depends on the heat energy generated by laser absorption on the powder surface. In addition, the beam quality deteriorates owing to the intrusion of metal vapor due to an increase in laser power. These factors can affect the surface distortion of the built structure. At a laser power of less than 60 W and a traverse speed of less than 20 mm/s, the surface distortion can be suppressed.

Fig. 10 displays the EPMA elemental mapping of the cross-section of the built structure fabricated at a laser power of 270 W and a traverse speed of 50 mm/s. The elements of pure copper and stainless steel were evenly mixed in the built structure. It has been reported that the Fe-Cu system does not form any intermetallic compounds, and there is a wide miscibility gap between Iron and Copper [27]. Because

cracks that failed to fuse on the centerline of the molten area were observed, it is considered that solidification cracking was induced. The molten area formed by laser irradiation is insufficient, which may cause cracks due to shrinkage during solidification from the liquid phase of the molten metal.

Figure 11 shows a 2D color plot of the percentage of crack generation. When the laser power and traverse speed were high, the percentage of crack generation increased. At high laser powers, the built height decreased owing to the excessive penetration depth, as depicted in Fig. 4. Meanwhile, the amount of powder supplied decreased with an increase in the traverse speed during the DED process. It is considered that there was a lack of molten metal to fill the central area of the surface where the liquid phase remained until the end of the solidification process. Cracks cannot be formed if the amount of molten metal is sufficient to reduce the tensile stress caused by shrinkage during solidification.

These results reveal that it is imperative to select a suitable laser power and traverse speed to obtain a high surface quality of the built structure without defects, such as meandering, distortion, and cracking.

3.4. Prediction of building conditions without surface defects

Figure 12 presents the prediction of a surface defect-free building condition at a powder feed rate of 20 mg/s. The continuous structure could not be formed owing to a lack of heat input at laser powers less than 60 W. The greater laser powers and traverse speeds contribute to meandering and cracks in the built structure. The amount of surface distortion in the built structure increased at a traverse speed of more than 20 mm/s. From these results, we can see that the built structure without surface defects can be obtained for laser powers between 60–270 W and traverse speeds of 10–20 mm/s.

4. Conclusions

This study focused on the DED-LB/M process using a pure copper powder. The influences of process parameters on distortion, meandering, and cracking, and defects of the built structure were investigated. The chemical composition of the cross-section of the built structure was analyzed using an electron probe microanalyzer (EPMA). The major results obtained are as follows:

1) The geometry of the built structure varied with building conditions. The laser power is a key factor that affects the built width and penetration depth, while the built height is dependent on the amount of powder supplied. The built height and width are inversely proportional to the traverse speed, but the penetration depth remains unaffected.

2) The distortion and meandering of the built structure may be induced by process instability due to the intrusion of metal vapor into the laser’s optical path. Meanwhile, cracks are formed due to shrinkage during solidification when the molten area formed by laser irradiation is insufficient. This indicates that it is important to select a suitable building condition to prevent these defects from occurring in the built structure.

3) Because the powder has a lower melting point than the substrate, thermal conduction from the molten metal of the substrate melts the powder. When the penetration size related to the heat capacity is small, the effect of thermal conduction from the molten metal of the substrate to the powder may weaken. This reveals that the absorption characteristics of the powder are a key factor affecting the melting of the powder and surface defects.
4) At a laser power of 60–270 W, and a traverse speed of 10–20 mm/s, a structure without surface defects could be obtained.

Declarations

Authors' contributions Mitsugu Yamaguchi organized all the data and wrote the manuscript. Masamichi Yamazaki investigated the building characteristics of the built structure in a single-line track during DED with a blue laser. Ayahito Saikai measured the geometry of the built structure. Yoshinori Funada and Taisei Yachi evaluated the quality of the structure built using EPMA. Tatsuaki Furumoto supervised all the research and analysis. All authors read and approved the final manuscript.

Funding Not applicable.

Availability of data and material All data generated or analyzed during this study are included in this published article.

Code availability Not applicable.

Ethics approval Not applicable.

Consent to participate Not applicable.

Consent for publish All authors consented to the publication.

Competing interests All authors declare that they have no competing.

References

1. Kar J, Roy SK, Roy GG (2016) Effect of beam oscillation on electron beam welding of copper with AISI-304 stainless steel. J Mater Process Technol 233:174–185. https://doi.org/10.1016/j.jmatprotec.2016.03.001
2. Sen I, Amankwah E, Kumar NS, Fleury E, Oh-ishi K, Hono K, Ramamurty U (2011) Microstructure and mechanical properties of annealed SUS 304H austenitic stainless steel with copper. Mater Sci Eng A 528:4491–4499. https://doi.org/10.1016/j.msea.2011.02.019
3. Espalin D, Muse DW, MacDonald E, Wicker RB (2014) 3D Printing multifunctionality: Structures with electronics. Int J Adv Manuf Technol 72:963–978. https://doi.org/10.1007/s00170-014-5717-7

4. Herzog D, Seyda V, Wycisk E, Emmelmann C (2016) Additive manufacturing of metals. Acta Mater 117:371–392. https://doi.org/10.1016/j.actamat.2016.07.019
5. Tran TQ, Chinnappan A, Lee JKY, Loc NH, Tran LT, Wang G, Kumar VV, Jayathilaka WADM, Ji D, Doddamani M, Ramakrishna S (2019) 3D printing of highly pure copper. Metals 9:756. https://doi.org/10.3390/met9070756
6. Zhang X, Sun C, Pan T, Flood A, Zhang Y, Li L, Liou F (2020) Additive manufacturing of copper-H13 tool steel bi-metallic structures via Ni-based multi-interlayer. Addit Manuf 36:101474. https://doi.org/10.1016/j.addma.2020.101474
7. Zhang X, Pan T, Chen Y, Li L, Zhang Y, Liou F (2021) Additive manufacturing of copper-stainless steel hybrid components using laser-aided directed energy deposition. J Mater Sci Technol 80:100–116. https://doi.org/10.1016/j.jmst.2020.11.048
8. Sun H, Chu X, Luo C, Chen H, Liu Z, Zhang Y, Zou Y (2021) Selective laser melting for joining dissimilar materials, Investigations of interfacial characteristics and in situ alloying. Metall Mater Trans A 52:1540–1550. https://doi.org/10.1007/s11661-021-06178-9
9. The Laser Society of Japan (1982) Laser Handbook, Ohmsha, Japan
10. Huang J, Yan X, Chang C, Xie Y, Ma W, Huang R, Zhao R, Li S, Liu M, Liao H (2020) Pure copper components fabricated by cold spray (CS) and selective laser melting (SLM) technology. Surf Coat Technol 395:125936. https://doi.org/10.1016/j.surfcoat.2020.125936
11. Adamson RS, Luzin V, Duguid A, Kannoorpatti K, Murray R (2020) Residual stress distributions in cold-sprayed copper 3D-printed parts. J Therm Spray Technol 29:1525–1537. https://doi.org/10.1007/s11666-020-01040-7
12. Hutasoit N, Rashid RAR, Palanisamy S, Duguid A (2020) Effect of build orientation and post-build heat treatment on the mechanical properties of cold spray additively manufactured copper parts. Int J Adv Manuf Technol 110:2341–2357. https://doi.org/10.1007/s00170-020-06010-5
13. Miyanaji H, Ma D, Atwater MA, Darling KA, Hammond VH, Williams CB (2020) Binder jetting additive manufacturing of copper foam structures. Addit Manuf 32:100960. https://doi.org/10.1016/j.addma.2019.100960
14. Miyanaji H, Rahman KM, Da M, Williams CB (2020) Effect of fine powder particles on quality of binder jetting parts. Addit Manuf 36:101587. https://doi.org/10.1016/j.addma.2020.101587
15. Bai Y, Williams CB (2015) An exploration of binder jetting of copper. Rapid Prototyp J 21:177–185. https://doi.org/10.1108/RPJ-12-2014-0180
16. Kumar A, Bai Y, Eklund A, Williams CB (2017) Effects of hot isostatic pressing on copper parts fabricated via binder jetting. Procedia Manuf 10:935–944. https://doi.org/10.1016/j.promfg.2017.07.084
17. Gargalis L, Ye J, Strantza M, Rubenchik A, Murray JW, Clare AT, Ashcroft IA, Hague R, Matthews MJ (2021) Determining processing behaviour of pure Cu in laser powder bed fusion using direct micro-calorimetry. J Mater Process Technol 294:117130. https://doi.org/10.1016/j.jmatprotec.2021.117130

18. Yadav S, Paul CP, Jinoop AN, Rai AK, Bindra KS (2020) Laser directed energy deposition based additive manufacturing of copper, Process development and material characterizations. J Manuf Process 58:984–997. https://doi.org/10.1016/j.jmapro.2020.09.008
19. Yadav S, Jinoop AN, Sinha N, Paul CP, Bindra KS (2020) Parametric investigation and characterization of laser directed energy deposited copper-nickel graded layers. Int J Adv Manuf Technol 108:3779–3791. https://doi.org/10.1007/s00170-020-05644-9
20. Yasuda K, Takada Y, Song JM (2021) Characterization of additively formed copper layer by blue laser-sintered copper nanoparticles. Proc Int Conf Electron Packag (ICEP) 53–54. https://doi.org/10.23919/ICEP51988.2021.9451986
21. Ono K, Sato Y, Higashino R, Funada Y, Abe N, Tsukamoto M (2021) Pure copper rod formation by multibeam laser metal deposition method with blue diode lasers. J laser Appl 33:012013. https://doi.org/10.2351/7.0000322
22. Asano K, Tsukamoto M, Sechi Y, Sato Y, Masuno S, Higashino R, Hara T, Sengoku M, Yoshida M (2018) Laser metal deposition of pure copper on stainless steel with blue and IR diode lasers. Opt Laser Technol 107:291–296. https://doi.org/10.1016/j.optlastec.2018.06.012
23. Li J, Cai Y, Yan F, Wang C, Zhu Z, Hu C (2020) Porosity and liquation cracking of dissimilar Nd:YAG laser welding of SUS304 stainless steel to T2 copper. Opt Laser Technol 122:105881. https://doi.org/10.1016/j.optlastec.2019.105881
24. Cheng H, Kang L, Wang C, Li Q, Chang B, Du D (2022) Dynamic behavior of molten pool backside during full-penetration laser welding of Ni-based superalloys. Int J Adv Manuf Technol. https://doi.org/10.1007/s00170-021-08187-9
25. Xie X, Zhou J, Long J (2021) Numerical study on molten pool dynamics and solute distribution in laser deep penetration welding of steel and aluminum. Opt Laser Technol 140:107085. https://doi.org/10.1016/j.optlastec.2021.107085
26. Yadroitsev I, Smurov I (2011) Surface morphology in selective laser melting of metal powders. Phys Proc A 12:264–270. https://doi.org/10.1016/j.phpro.2011.03.034
27. Shi RP, Wang CP, Wheeler D, Liu XJ, Wang Y (2013) Formation mechanisms of self-organized core/shell and core/shell/corona microstructures in liquid droplets of immiscible alloys. Acta Mater 61:1229–1243. https://doi.org/10.1016/j.actamat.2012.10.033

Figures

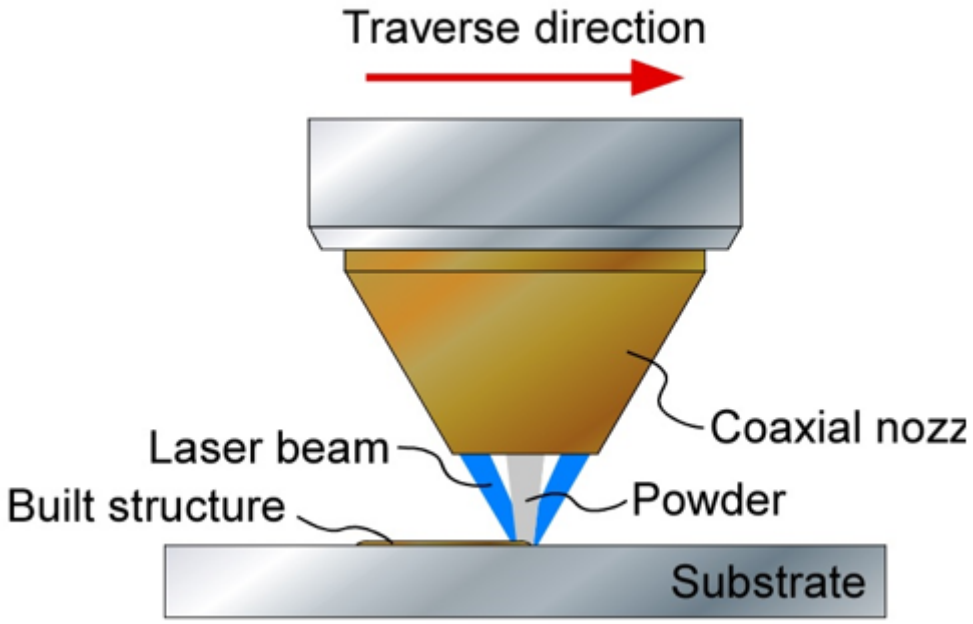

Figure 1

Schematic of the experimental setup

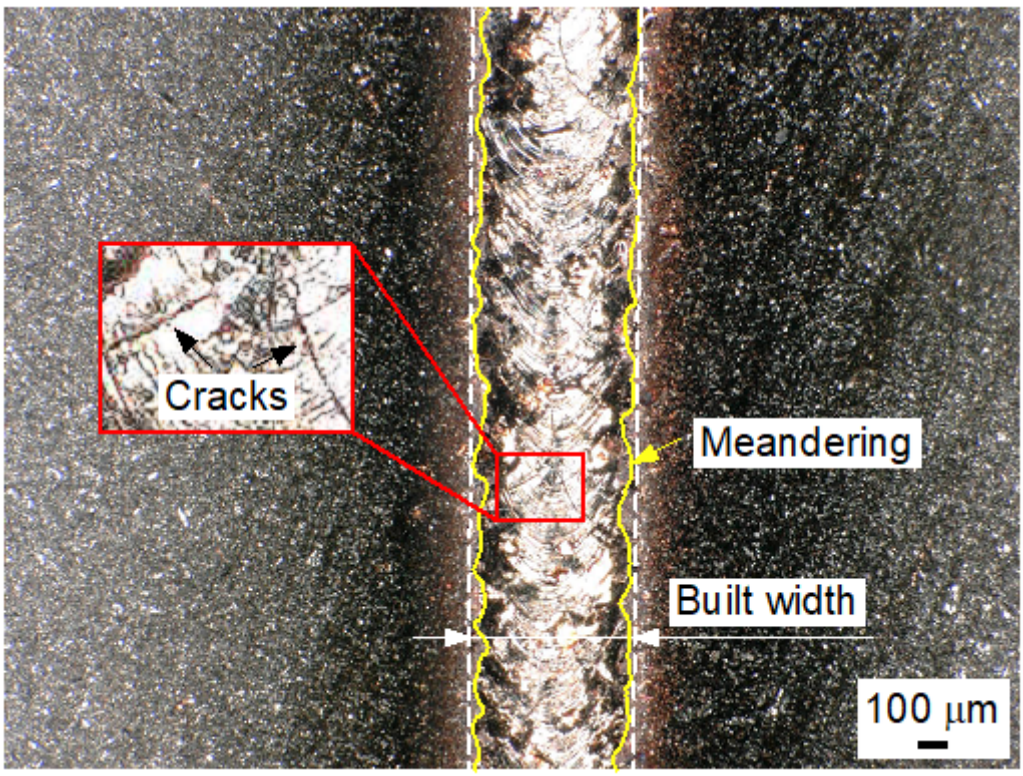

Figure 2

Evaluation of built width and defects such as meandering and cracking in the built structure

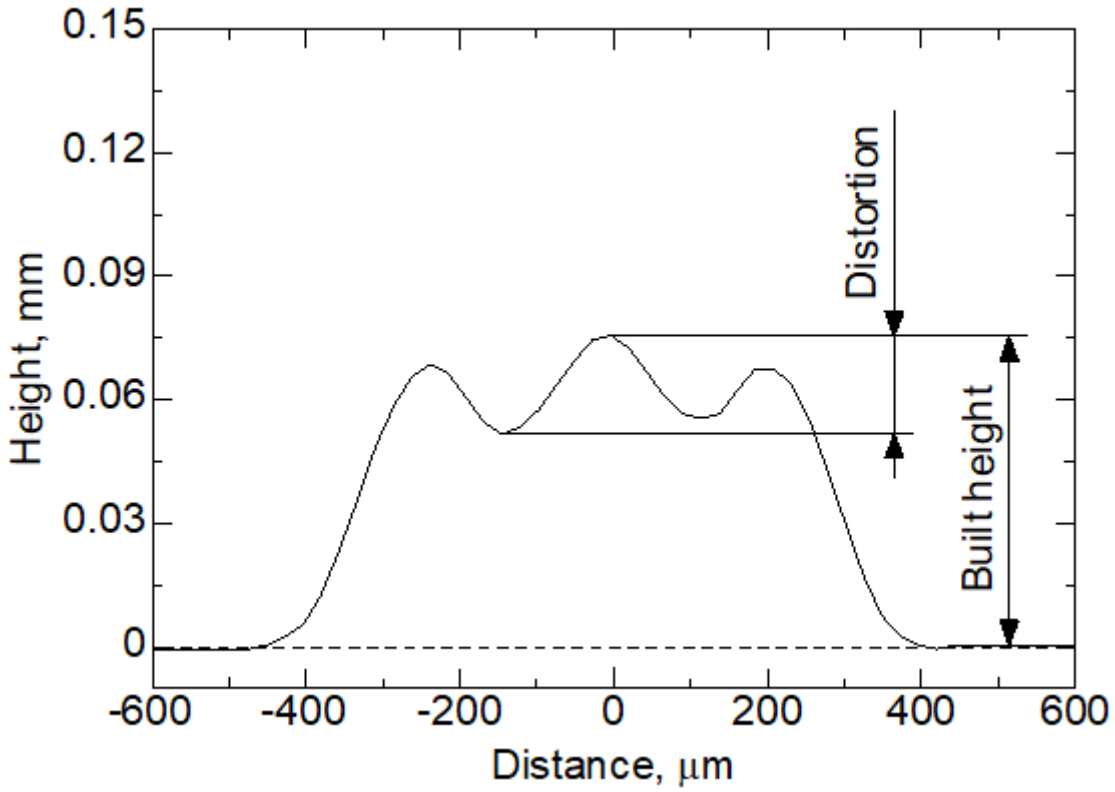

Figure 3

Evaluation of built height and defects such as surface distortion in the built structure

Figure 4

Variations in the built heights, widths, and penetration depths under various laser powers

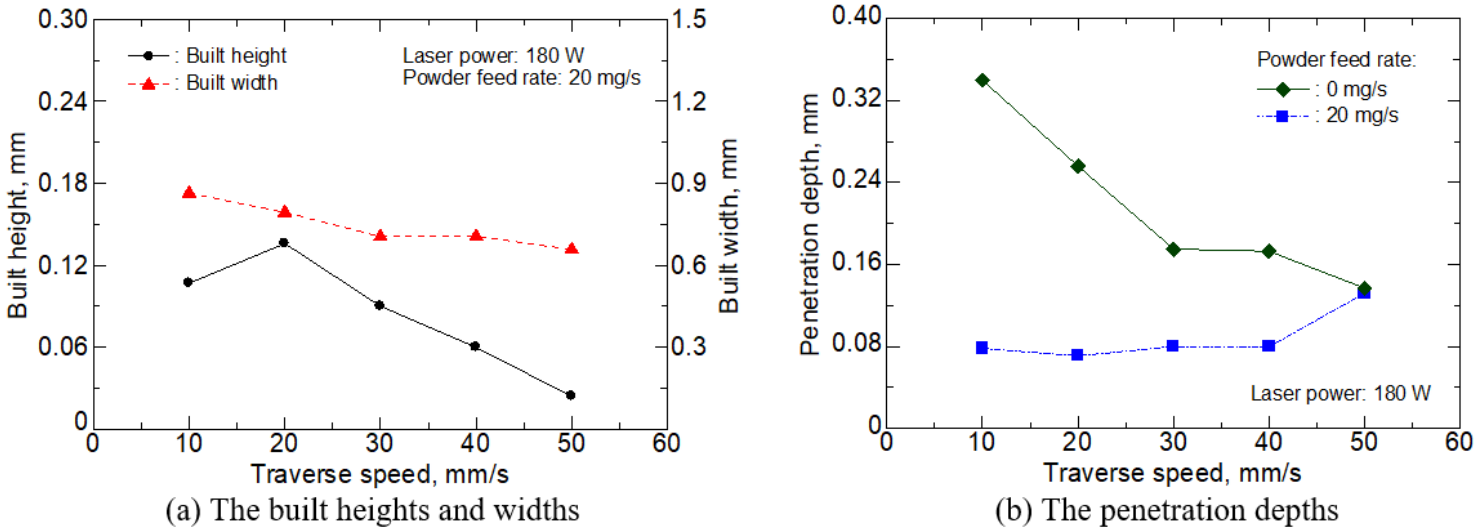

Figure 5

Variation in the built heights, widths, and penetration depths at various traverse speeds

Figure 6

Appearance of the built structures fabricated at the traverse speed of 40 mm/s under different laser powers

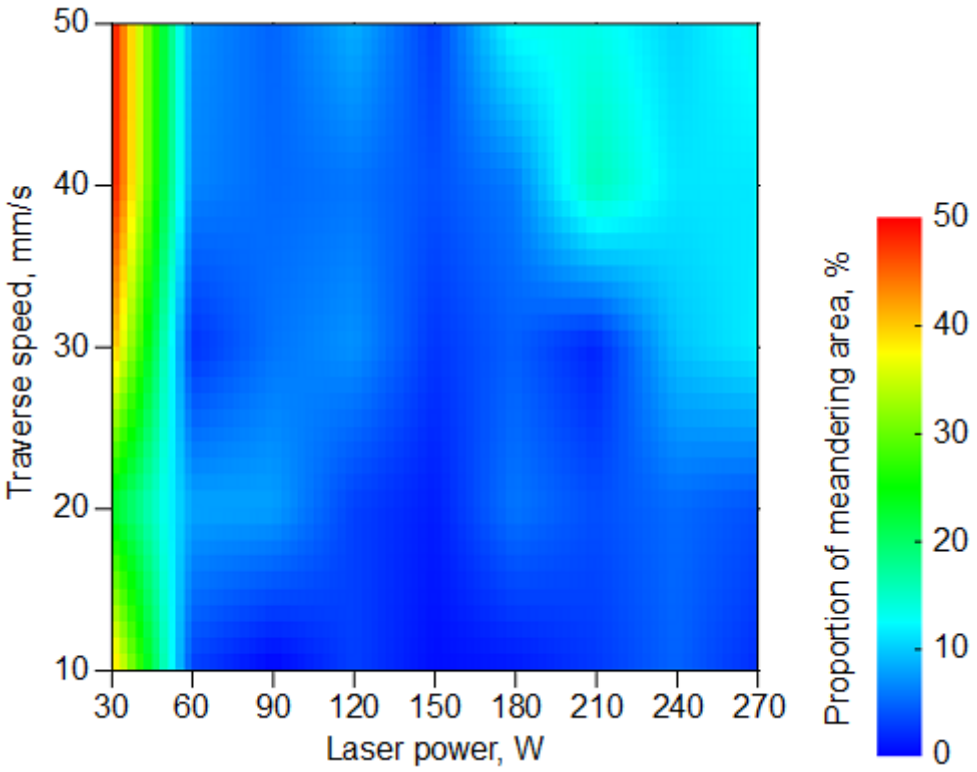

Figure 7

Proportion of meandering area in the built structure

Figure 8

Cross-sectional profiles of the built structures fabricated at the laser power of 180 W under different traverse speeds

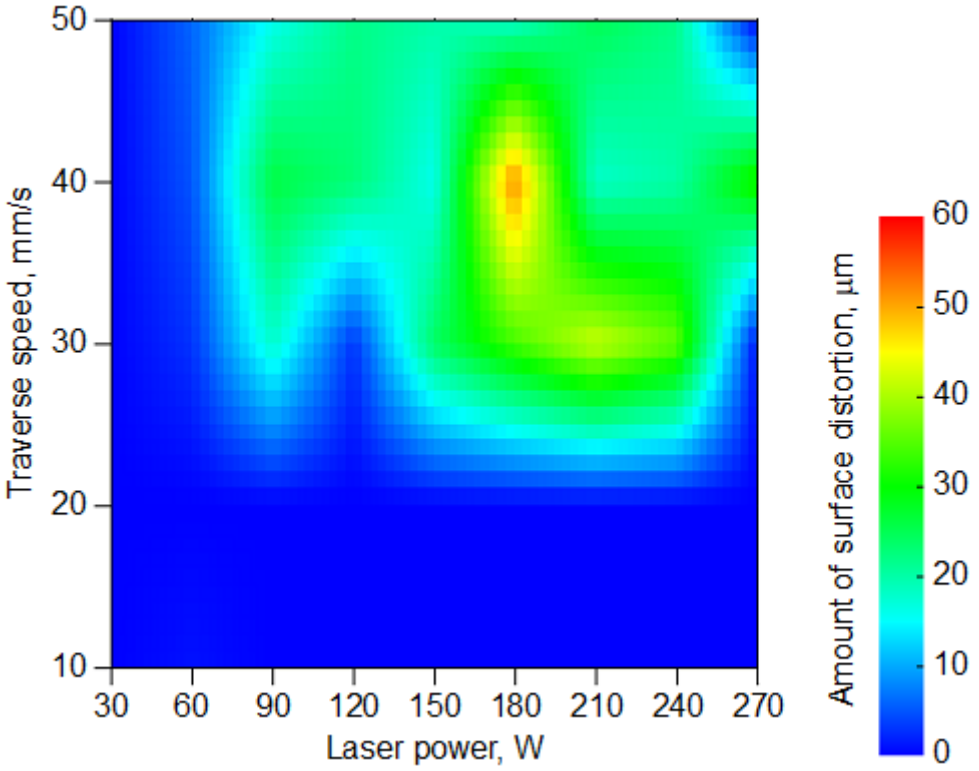

Figure 9

Amount of surface distortion in the built structure

Figure 10

EPMA elemental mapping of cross-section of the built structure fabricated at the laser power of 270 W and the traverse speed of 50 mm/s

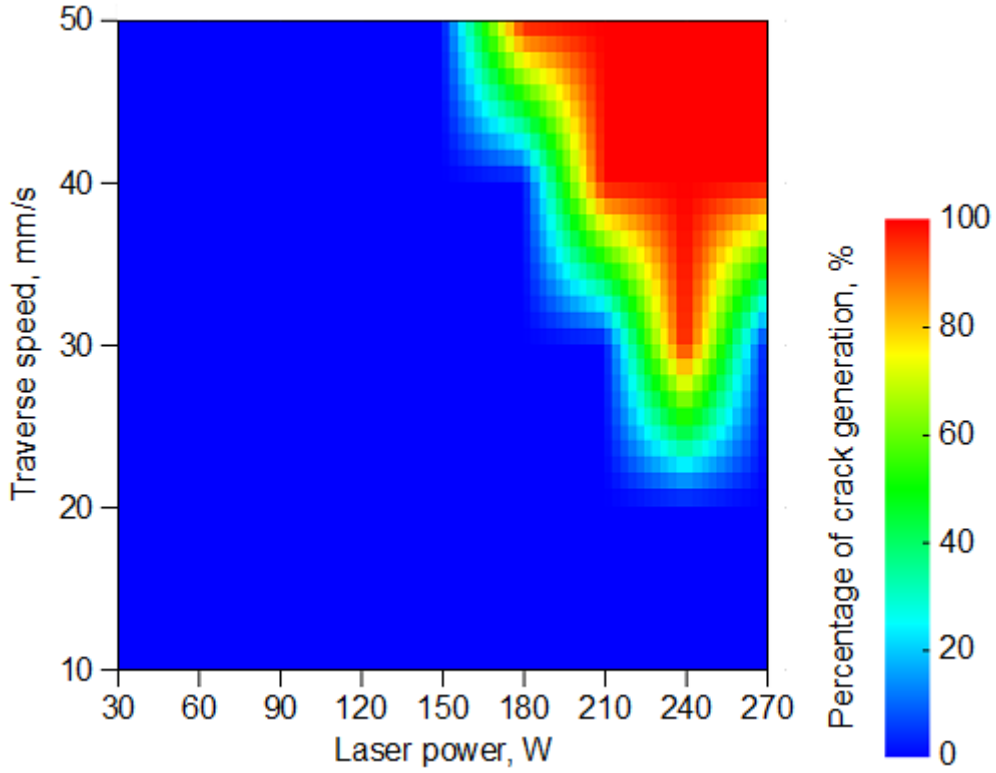

Figure 11

Percentage of crack generation

Figure 12

Prediction of surface defect-free building conditions